

# Modulating Photostability and Mitochondria Selectivity in Far-Red/NIR Emitting Coumarin Fluorophores through Replacement of Pyridinium by Pyrimidinium

Anna Rovira, Miriam Pujals, Albert Gandioso, Marta López-Corrales, Manel Bosch, and Vicente Marchán\*



Cite This: <https://dx.doi.org/10.1021/acs.joc.0c00570>



Read Online

ACCESS |



Metrics & More

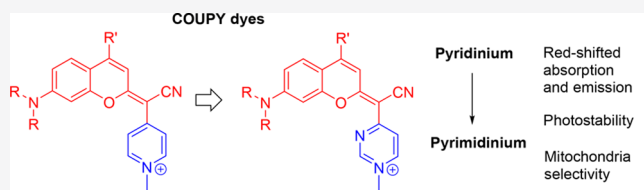


Article Recommendations



Supporting Information

**ABSTRACT:** Mitochondrial dysfunction has been associated with several human pathological conditions, including cancer, aging, and neurodegenerative diseases. Thus, the availability of selective fluorescent probes for mitochondria could play an important role in the future for monitoring cellular functions and disease progression. In this work, we have studied how the photophysical properties and subcellular accumulation of nonconventional coumarin-based COUPY fluorophores can be fine-tuned through replacement of the *para*-pyridinium moiety with several heterocycles. Among them, *ortho,para*-pyrimidinium substitution provided novel fluorophores with suitable photophysical properties for bioimaging applications, including emission in the far-red to NIR region, large Stokes' shifts, and high photostability. Furthermore, the compounds exhibited excellent cell membrane permeability in living cells and a higher selectivity for mitochondria compared with the parent COUPY fluorophores. Overall, these results provided useful insights into the development of novel mitochondria-targeted fluorescent probes based on small organic molecules, since higher selectivity for this organelle can be achieved through the replacement of conventional N-alkylated pyridinium moieties by the corresponding N-alkylated-*ortho,para*-pyrimidinium counterparts.



## INTRODUCTION

Fluorescence imaging in combination with organic fluorophores has become a powerful tool for understanding biological events at a molecular level. In this context, the use of fluorescent probes with operability in the less energetic far-red and near-infrared (NIR) region of the electromagnetic spectrum offers several appealing features for in vivo imaging applications, such as increased tissue penetration depth and minimal autofluorescence interference from natively occurring biomolecules.<sup>1</sup> For this reason, recent efforts have been devoted to the development of novel organic chromophores operating in the phototherapeutic window with optimal photophysical (e.g., long-wavelength absorption and emission, brightness, large Stokes' shifts, and photostability) and physicochemical (e.g., aqueous solubility, good cell permeability, and target specificity) properties. Ideally, such fluorescent compounds should be based on chemically stable, low molecular weight scaffolds amenable to smart and simple structural modifications to fine-tune the abovementioned properties and to facilitate conjugation to targeting ligands.<sup>2</sup> Besides biocompatibility, an ideal fluorophore should permit the interrogation of intracellular architectures and dynamics without disturbing and compromising the integrity of the cellular target.<sup>3</sup>

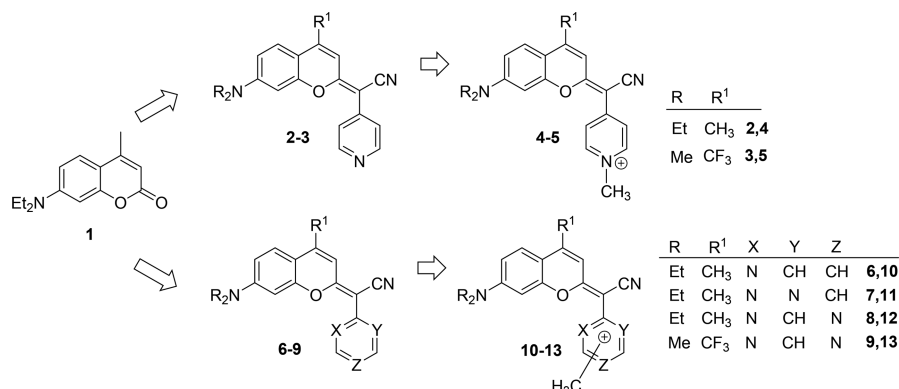
Mitochondria are involved in many key cellular processes, including ATP synthesis, calcium signaling, and redox

homeostasis.<sup>4</sup> Mitochondrial dysfunction has been associated with a wide range of human pathological conditions, such as cancer disease, aging, and metabolic and neurodegenerative diseases.<sup>5</sup> Thus, the availability of fluorescent dyes that can selectively stain mitochondria opens the door to monitoring cellular functions and disease progression by studying mitochondrial morphology and mitophagy.<sup>6</sup> Among fluorescent mitochondrial probes described to date, some of them intrinsically target this organelle such as some cyanine derivatives (e.g., IR-780 and MHI-148) and some rhodamines (Rhodamine 123).<sup>7</sup> Another approach to achieve mitochondria selectivity consists of incorporating lipophilic positively charged moieties such as triphenylphosphonium or pyridinium groups, which exploit the negative potential across the outer and inner mitochondrial membrane.<sup>8</sup> In this context, anticancer mitochondria-targeted fluorescent molecules are considered attractive theranostic agents.<sup>9</sup> Similarly, mitochondria-targeted photocages based on organic chromophores

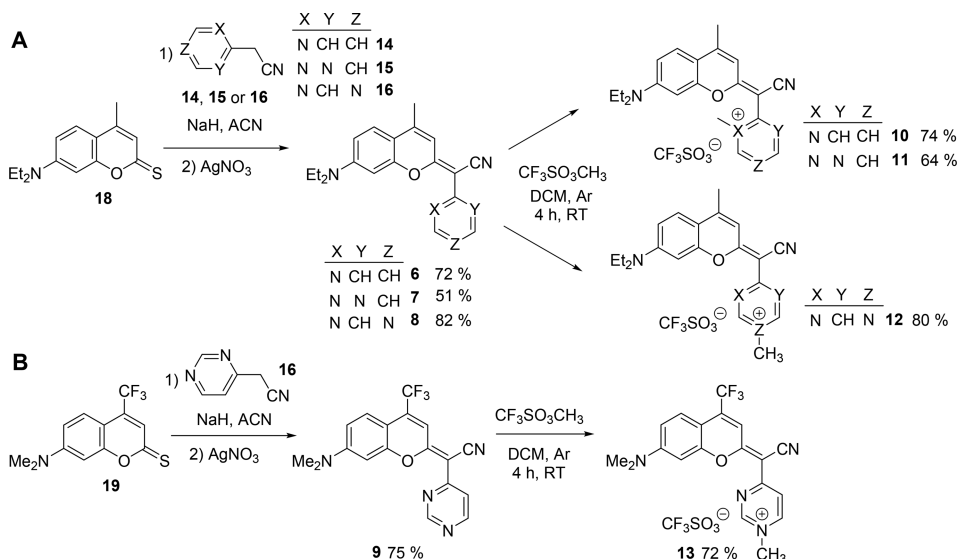
Received: March 3, 2020

Published: April 2, 2020

## Scheme 1. Rational design of novel COUPY fluorophores



## Scheme 2. Synthesis of COUPY scaffolds (6–9) and the corresponding N-methylated dyes (10–13)



provide a powerful method for releasing bioactive compounds within this organelle.<sup>10</sup>

In our laboratory, we have recently described a new class of coumarin-based chromophores in which the carbonyl group of the electron-withdrawing lactone in conventional coumarin **1** was replaced by the cyano(4-pyridine)methylene moiety (e.g., compounds **2** and **3**; see Scheme 1) with the aim of increasing the push-pull character of the  $\pi$ -delocalized system.<sup>11</sup> N-Alkylation of the pyridine heterocycle provides low molecular weight fluorophores, nicknamed COUPYs, with several attractive characteristics, including emission in the far-red/NIR region, large Stokes' shifts, and good brightness.<sup>11</sup> Moreover, COUPY dyes (e.g., see compounds **4** and **5** in Scheme 1 as representative examples) exhibited moderate to good aqueous solubility and excellent cell membrane permeability and accumulated preferentially in two specific cellular compartments, the mitochondria and nucleoli. After the discovery of this promising fluorescent platform, we have initiated a systematic study to unveil the principles governing the structure-photophysical property relationships (SPPR) of COUPY dyes, which are necessary to design new fluorescent probes as per need. Compared with conventional coumarins (e.g., **1**), the molecular framework of COUPY scaffolds offers several advantages for carrying out a systematic SPPR study. Indeed, we have found that absorption and emission maxima

can be red-shifted through the incorporation of strong electron-withdrawing groups like CF<sub>3</sub> either at the 4-position or via N-alkylation of the pyridine heterocycle,<sup>11</sup> while photostability can be increased through replacement of the electron-donating *N,N*-dialkyl groups (e.g., NMe<sub>2</sub> or NEt<sub>2</sub>) at position 7 with azetidine.<sup>12</sup> In addition, conjugatable versions of COUPY dyes can be easily obtained by incorporation of suitable functional groups (e.g., carboxylic acid, amino, azide, or alkyne) via N-alkylation of the pyridine moiety. Such COUPY derivatives allowed us to label receptor-binding peptides on a solid phase by using efficient click chemistry methodologies<sup>13</sup> and to develop novel photosensitizers for photodynamic anticancer therapy via conjugation to cyclometalated Ir(III) complexes.<sup>14</sup>

On the basis of all these precedents, in this work we focused on investigating how the modification of the pyridine moiety in COUPY chromophores could influence the photophysical properties and subcellular accumulation of the compounds. With this idea in mind, herein we describe the synthesis and characterization of four analogues (compounds **10–13**, Scheme 1) of our original COUPY dyes (**4** and **5**). Surprisingly, the replacement of the *para*-pyridine heterocycle by *ortho*-pyridine (**10**) or *ortho,ortho*-pyrimidine (**11**) had a negative effect on the spectroscopic properties of the compounds since both absorption and emission were blue-

shifted. By contrast, the incorporation of *ortho,para*-pyrimidine (12 and 13) led to highly photostable fluorophores with improved photophysical properties compared with that of the parent compounds, including emission in the far-red to NIR region and large Stokes's shifts. Furthermore, high cell permeability was retained in both *ortho,para*-pyrimidine-containing dyes and a higher selectivity for mitochondria of HeLa cells was achieved. Overall, these results provided new insights into the design and optimization of mitochondria-targeted fluorescent probes.

## RESULTS AND DISCUSSION

**Design, Synthesis, and Characterization of COUPY Dyes.** COUPY dyes 10–13 were synthesized by following our previously described methodology for the parent dyes (4 and 5), which is based on the reaction of a thiocoumarin precursor with suitable heteroarylacetonitrile derivatives followed by N-methylation of the pyridine or pyrimidine moieties (Scheme 2). First, thiocoumarin 18<sup>15</sup> was reacted with 2-(pyridin-2-yl)acetonitrile (14), 2-(pyrimidin-2-yl)acetonitrile (15), or 2-(pyrimidin-4-yl)acetonitrile (16) in the presence of NaH followed by AgNO<sub>3</sub> treatment, which afforded COUPY scaffolds 6, 7, and 8, respectively, after purification by silica column chromatography with moderate to good yields (51–82%). Similarly, coumarin 9 was obtained by condensation of thiocoumarin 19<sup>11</sup> with 16 (yield 75%). All the compounds were fully characterized by reversed-phase high-performance liquid chromatography (HPLC) (Figure S1), HR ESI-MS, and <sup>1</sup>H, <sup>19</sup>F (only in the case of 9), and <sup>13</sup>C NMR.

It is worth noting that <sup>1</sup>H-<sup>1</sup>H NOESY experiments (Figure 1 and Figures S2–S5) account for the existence of two species in equilibrium in solution because of the rotation around the exocyclic C=C bond, which reproduces the behavior previously found in the parent COUPY scaffolds (compounds 2 and 3, Scheme 1).<sup>11</sup> As shown in Figure 1, chemical

exchange cross-peaks between the resonances of *E* and *Z* rotamers were observed in the 2D NOESY spectrum of coumarin 8. In the case of coumarins 6, 8, and 9, the two rotamers were present in a ~60:40 ratio according to the integration of the <sup>1</sup>H NMR spectrum, the *E* rotamer being the major species. This is in contrast with the *para*-pyridine-containing coumarins 2 and 3 in which the *E/Z* ratio was ~90:10. Surprisingly, the *Z* rotamer was the major species in solution (95%) in the COUPY scaffold containing the *ortho,ortho*-pyrimidine heterocycle (7), which was confirmed by the existence of a NOE cross-peak between the proton at position 3 of the coumarin moiety and the proton at the *ortho* position of the pyrimidine ring (Figure S3). It is worth noting that in all of the COUPY scaffolds the chemical shift of H3 appears at higher  $\delta$  in the *Z* isomer (e.g., 8.18 ppm in 7 and 8.26 ppm in 8) than in the *E* isomer (e.g., 6.70 ppm in 7 and 6.75 ppm in 8).

Next, we synthesized the corresponding N-methylated pyridinium (10) and pyrimidinium (11–13) dyes by reaction with methyl trifluoromethanesulfonate in DCM at room temperature.<sup>11</sup> The four new coumarin derivatives were isolated after silica column chromatography as reddish-orange (10 and 11), purple (12), and dark blue (13) solids (yields 64–80%), and their purity was assessed by reversed-phase HPLC (Figure S1). Characterization was carried out by HR ESI-MS and 1D and 2D NMR spectroscopy. As expected, methylation occurred at the less sterically hindered nitrogen in the *ortho,para*-pyrimidine derivatives (12 and 13) according to NOESY NMR characterization, and in all cases the *E* rotamer was the major species in solution (Figures S6–S9).

**Photophysical Characterization of COUPY Fluorophores.** Having at hand COUPY dyes 10–13, we investigated the effect of replacing the *para*-pyridine moiety in the parent fluorophores (4 and 5) by the *ortho*-pyridine or *ortho,ortho*- or *ortho,para*-pyrimidine on the spectroscopic and photophysical properties of the compounds with the aim of establishing new SPPR. Although water or phosphate buffered saline (PBS) is often used to evaluate the usefulness of a new fluorophore within a spectroscopy cuvette, the heterogeneity and complexity of the cellular environment cannot be accurately described by using a simple aqueous buffer.<sup>16</sup> For this reason, we decided to register the UV–vis absorption and emission spectra in four solvents of different polarities (PBS buffer pH 7.4, EtOH, ACN, and DCM; Figure 2 and Figures S10–S17) to get some

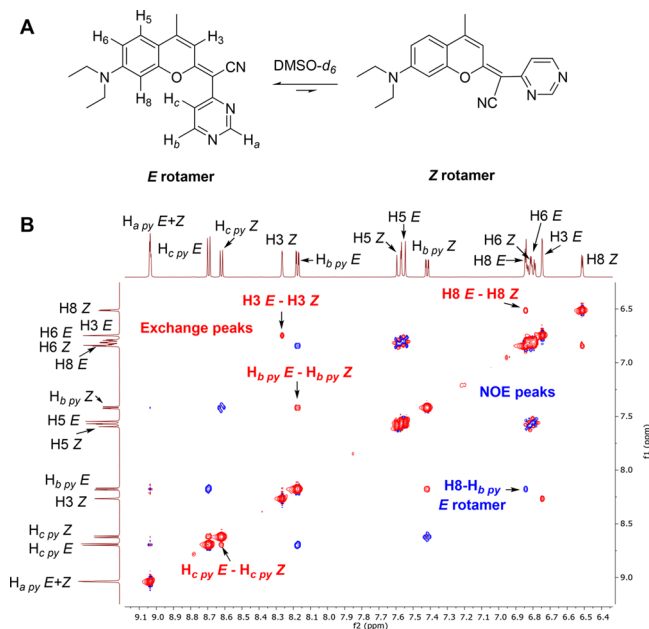


**Figure 1.** (A) Structures of the *E* and *Z* rotamers of coumarin 8. (B) Expansion of the 2D NOESY spectrum ( $t_m = 500$  ms, 25 °C) of 8 in DMSO- $d_6$  showing NOE cross-peaks and exchange cross-peaks between rotamer resonances of the same sign as the diagonal.

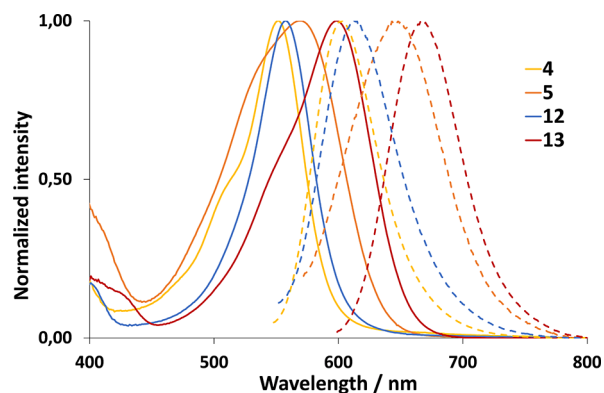
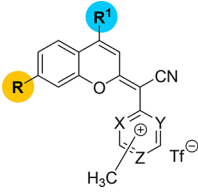


**Figure 2.** Comparison of the normalized absorption (solid lines) and fluorescence (dotted lines) spectra of COUPY dyes (compounds 4, 5, 12, and 13) in EtOH.

Table 1. Photophysical Data of the Coumarin Derivatives 4 and 5 and 10–13 in Different Solvents



$R = -\frac{1}{2}-NEt_2$  (4,10–12)  $-\frac{1}{2}-NMe_2$  (5,13)  
 $R' = CH_3$  (4,10–12),  $CF_3$  (5,13)

compd.	X, Y, Z	solvent	$\lambda_{abs}$ (nm) <sup>a</sup>	$\epsilon$ (M <sup>-1</sup> cm <sup>-1</sup> ) <sup>b</sup>	$\lambda_{em}$ (nm) <sup>c</sup>	Stokes shift (nm) <sup>d</sup>	$\Phi_F$ <sup>e</sup>
4	CH, CH, N	PBS	545	34,000	604	59	0.12
		EtOH	552	59,000	603	51	0.45
		ACN	548	75,000	609	61	0.18
		DCM	569	67,000	607	38	0.70
10	N, CH, CH	PBS	502	25,000	583	81	0.01
		EtOH	515	31,000	592	77	0.02
		ACN	505	26,000	589	84	0.02
		DCM	543	36,000	594	51	0.20
11	N, N, CH	PBS	525	37,000	561	36	0.01
		EtOH	528	59,000	564	36	0.11
		ACN	526	23,000	575	49	0.02
		DCM	551	45,000	565	14	0.02
12	N, CH, N	PBS	557	56,000	628	71	0.01
		EtOH	558	58,000	615	57	0.13
		ACN	557	50,000	621	64	0.10
		DCM	575	73,000	618	43	0.11
5	CH, CH, N	PBS	568	14,000	660	92	0.02
		EtOH	568	20,000	648	80	0.05
		ACN	569	47,000	668	99	0.02
		DCM	600	34,000	657	57	0.05
13	N, CH, N	PBS	600	35,000	673	73	0.02
		EtOH	598	58,000	667	69	0.08
		ACN	597	42,000	674	77	0.10
		DCM	624	60,000	663	39	0.41

<sup>a</sup>Wavelength of the absorption maximum. <sup>b</sup>Molar absorption coefficient at  $\lambda_{max}$ . <sup>c</sup>Wavelength of the emission maximum upon excitation at a wavelength 20 nm below  $\lambda_{max}$ . <sup>d</sup>Stokes' shift. <sup>e</sup>Fluorescence quantum yields ( $\Phi_F$ ) were measured by a comparative method using cresyl violet in ethanol ( $\Phi_{F,Ref} = 0.54$ ) as a reference for compounds 4, 5, 12, and 13. Fluorescein dissolved in aqueous sodium hydroxide (0.1 M;  $\Phi_{F,Ref} = 0.92$ ) was used as a reference in the case of compounds 10 and 11.<sup>17</sup>

insights into the photophysical behavior of the compounds in polar and less-polar environments. As shown in Table 1, the photophysical properties of coumarins 10–13 were compared with those of the parent compounds 4 and 5<sup>11</sup> to facilitate the establishment of SPPR.

All the new compounds exhibited an intense absorption band in the visible region of the electromagnetic spectrum, with the absorption maxima ranging from 502 nm (10) to 600 nm (13) in aqueous solution (PBS pH 7.4) and from 543 nm (10) to 624 nm (13) in DCM. To our surprise, the absorption maximum of coumarin 10 was significantly blue-shifted with respect the reference compound 4 (e.g., compare  $\lambda_{abs} = 515$  and 543 nm for 10 and  $\lambda_{abs} = 552$  and 569 nm for 4 in EtOH and DCM, respectively). Although not as pronounced as in the case of 10, a similar trend was found in *ortho,ortho*-pyrimidine-containing coumarin (11) since its absorption maximum was also blue-shifted (18–24 nm depending on the solvent) with respect 4. By contrast, a slight red shift was found in the absorption maximum of the *ortho,para*-pyrimidine-containing coumarin 12 (12 nm in PBS and 6 nm in DCM). This red-shift was considerably larger in the 4- $CF_3$  analogue (e.g., compare  $\lambda_{abs} = 600$  nm for 13 and  $\lambda_{abs} = 568$  nm for 5 in PBS). As previously observed with the first generation of COUPY dyes,<sup>11,12</sup> 10–13 showed negative solvatochromism since the

absorption maxima was blue-shifted with increasing polarity of the solvent (e.g., compare the  $\lambda_{abs}$  of 10–13 in DCM with the corresponding values in aprotic (ACN) and protic (EtOH) polar solvents). Moreover, the molar absorption coefficients of the two derivatives containing the *ortho,para*-pyrimidine moiety were similar to or even higher than those of their respective parent dyes, especially in the 4- $CF_3$  analogue (e.g., compare  $\epsilon = 58$  mM<sup>-1</sup> cm<sup>-1</sup> for 13 and  $\epsilon = 20$  mM<sup>-1</sup> cm<sup>-1</sup> for 5 in EtOH).

The emission maxima of coumarins 10 and 11 were also blue-shifted both in polar and less-polar solvents with respect coumarin 4 (e.g.,  $\lambda_{em} = 564$  nm for 11 and  $\lambda_{em} = 603$  nm for 4 in EtOH), which reproduces the effect of replacing *para*-pyridine by *ortho*-pyridine or *ortho,ortho*-pyrimidine moieties on the compounds' absorption maxima. By contrast, the emission maxima of COUPY dyes containing the *ortho,para*-pyrimidine moiety was red-shifted with respect to that of their parent compounds (11–24 nm in 12 and 6–19 nm in 13), especially in polar solvents. As a consequence, COUPY dyes 12 and 13 showed emission in the far-red to NIR region (Figure 2 and Figures S10–S17), the emission maximum in polar media being particularly appealing in the case of the 4- $CF_3$  fluorophore ( $\lambda_{em} = 673$  nm for 13 in PBS). Interestingly, coumarin 12 exhibited larger Stokes' shifts than its parent dye



4 in all the solvents evaluated, while the replacement of *para*-pyridine by *ortho,para*-pyrimidine in **5** led to slightly lower values. Nevertheless, the Stokes' shifts of **12** and **13** in polar solvents are sufficiently large (e.g., 71 and 73 nm in PBS, respectively) to avoid the light reabsorption problems typically found in bioimaging applications.<sup>1</sup>

As shown in Table 1, compounds **10** and **11** exhibited very weak fluorescence in all the solvents investigated. By contrast, fluorescence quantum yields for coumarin **13** were much higher than those of the parent compound **5**, especially in less-polar solvents (e.g., 0.41 and 0.05 in DCM, respectively). This tendency was reversed in the case of the 4-CH<sub>3</sub> analogue since the  $\Phi_F$  for **12** was smaller compared with that of **4** (e.g., 0.11 and 0.70 in DCM, respectively). Both *ortho,para*-pyrimidine-containing compounds exhibited moderate fluorescence quantum yields in polar protic solvents ( $\Phi_F = 0.13$  for **12** and  $\Phi_F = 0.08$  for **13** in EtOH).

Finally, the photostability of the most promising coumarins (**12** and **13**) was investigated in PBS buffer (pH 7.4) under green LED irradiation (Figure 3 and Figure S18). As shown in

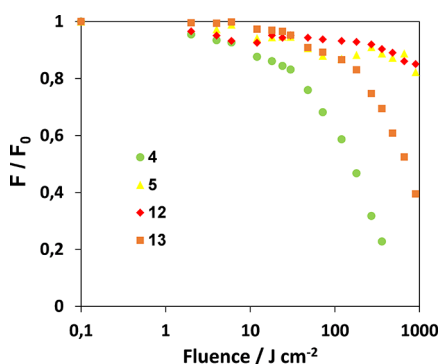


**Figure 3.** Fluorescence bleaching of COUPY dyes (**4**, **5**, **12**, and **13**) in PBS buffer pH 7.4 (5  $\mu$ M) irradiated with green light (505 nm, 100 mW/cm<sup>2</sup>).

Figure 3, the replacement of pyridine in coumarin **4** with *ortho,para*-pyrimidine had a positive effect on the photostability of the resulting fluorophore (**12**). By contrast, coumarin **13** was found less photostable than its parent compound **5** and coumarin **12**, which indicates that replacement of the CH<sub>3</sub> group at the 4-position with CF<sub>3</sub> in *ortho,para*-pyrimidine-containing COUPY dyes does not lead to an improvement of the overall photostability of the compounds. Nevertheless, it is worth noting that the two new pyrimidine-containing COUPY dyes were found photostable up to light fluences larger than 1000 J/cm<sup>2</sup> (**12**) and 200 J/cm<sup>2</sup> (**13**), which are more than 50- and 10-fold, respectively, higher than those typically used in imaging experiments with living cells.

In summary, all these observations allowed us to establish some SPPR. First, replacement of *para*-pyridine in COUPY dyes with *ortho*-pyridine or *ortho,ortho*-pyrimidine moieties had a negative effect on the spectroscopic properties of the fluorophores since both absorption and emission maxima were blue-shifted. Moreover, compounds **10** and **11** were found to be weakly fluorescent and their extinction coefficients were smaller than those of the parent coumarin **4**. By contrast, the photophysical properties of COUPY dyes were clearly improved when *para*-pyridine was replaced with *ortho,para*-pyrimidine. On the one hand, both absorption and emission

maxima were red-shifted with respect to that of the parent compounds, especially in polar protic solvents. Indeed, the incorporation of the second nitrogen atom in the pyridine moiety in **5** caused a red shift of the absorption (32 nm) and emission (12 nm) bands in PBS pH 7.4 in the resulting coumarin **13** when compared with the parent compound. Very interestingly, the emission of **13** was extended beyond 750 nm (Figure 2), which would facilitate in vivo imaging. Although the incorporation of the *ortho,para*-pyrimidine moiety caused a slight decrease in the fluorescence quantum yields of the compounds (e.g., compare  $\Phi_F$  of **4** and **12**), the combination of this heterocycle with the CF<sub>3</sub> group at position 4 seems to compensate for this phenomenon, leading to moderate  $\Phi_F$  values in protic and aprotic polar solvents (0.08–0.13) in the case of compound **13**.

#### Fluorescence Imaging of COUPY Dyes in Living Cells.

Taking into account the large photostability and the photophysical properties of the two *ortho,para*-pyrimidine-containing COUPY dyes (**12** and **13**), we decided to evaluate their usefulness as fluorescent probes in a more realistic situation (e.g., in living cells). As previously stated, the heterogeneous environment of an organic fluorophore within a cell or within a specific cellular organelle might be considerably different than the homogeneity of a solution in a spectroscopy cuvette. In fact, the presence of biomolecules such as proteins and lipids or the interaction with the components of cellular membranes might provide the fluorescent probe with an environment less hydrophilic than expected, thereby modifying the key parameters for bioimaging applications such as brightness.

The cellular uptake of **12** and **13** was first investigated in living HeLa cells (2  $\mu$ M, 30 min incubation) by using confocal microscopy and compared with that of the *para*-pyridine-containing coumarins (compounds **4** and **5**, respectively). Irradiation was carried out with a yellow light laser ( $\lambda_{ex} = 561$  nm) in the case of 4-CH<sub>3</sub> coumarins (**4** and **12**), while the higher red-shift absorption of the 4-CF<sub>3</sub> compounds (**5** and **13**) allowed the use of a red one ( $\lambda_{ex} = 633$  nm). As shown in Figure 4, in all cases the fluorescence signal was clearly observed inside the cell, which confirms that the excellent cellular uptake of the parent COUPY dyes was retained after replacement of pyridine with pyrimidine. In addition, it is worth noting that no cell toxicity was observed during these studies. The overall pattern of staining (but not the relative fluorescence intensity between organelles; see below for a discussion) of pyrimidine-containing coumarins (**12** and **13**) was similar to that found with the parent fluorophores (**4** and **5**), suggesting accumulation in mitochondria, nucleoli and, to a lesser extent, in intracellular vesicles, mostly lysosomes. Colocalization experiments with two specific markers for labeling mitochondria (MitoTracker Green FM, MTG) and lysosomes (LysoTracker Green FM, LTG) confirmed the subcellular localization of the compounds.

As shown in Figure 5, the distribution of the fluorescence emission of the compounds was similar to that of MitoTracker Green FM, which confirmed accumulation into the mitochondria. Pearson's and Manders' ( $M_1$  and  $M_2$ ) coefficients were used to measure the degree of colocalization.<sup>11,12,18</sup> On the one hand, Pearson's coefficients of 0.86 (**12**) and 0.87 (**13**) confirmed a clear correlation between the coumarin signals and MTG (Pearson's coefficients ranging from  $-1$  to  $+1$ ,  $+1$  being the indicator of a perfect match). Such coefficients were higher than those obtained for the parent COUPY dyes (0.65 for **4** and 0.73 for **5**), indicating a better correlation between

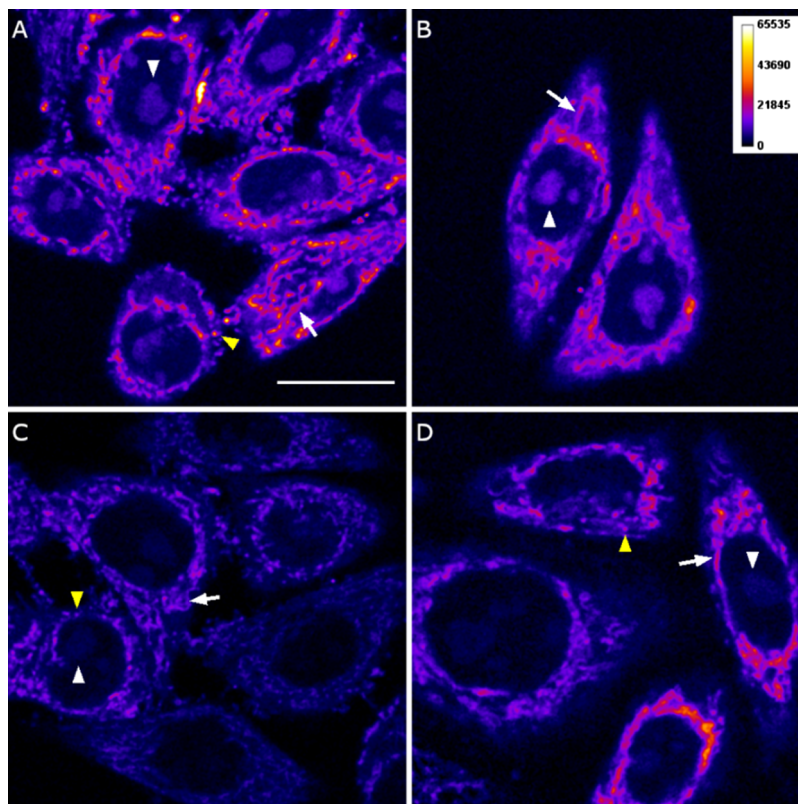


**Figure 4.** Cellular uptake of COUPY fluorophores (A) 4, (B) 5, (C) 12, and (D) 13. Single confocal planes of HeLa cells incubated with the compounds ( $2\ \mu\text{M}$ , 30 min,  $37\ ^\circ\text{C}$ ). White arrows point out mitochondria, white arrowheads nucleoli, and yellow arrowheads stained vesicles. Scale bar:  $20\ \mu\text{m}$ . All images are at the same scale as (A) and color coded using the Fire lookup table from Fiji (intensity calibration bar is showed in (B)).

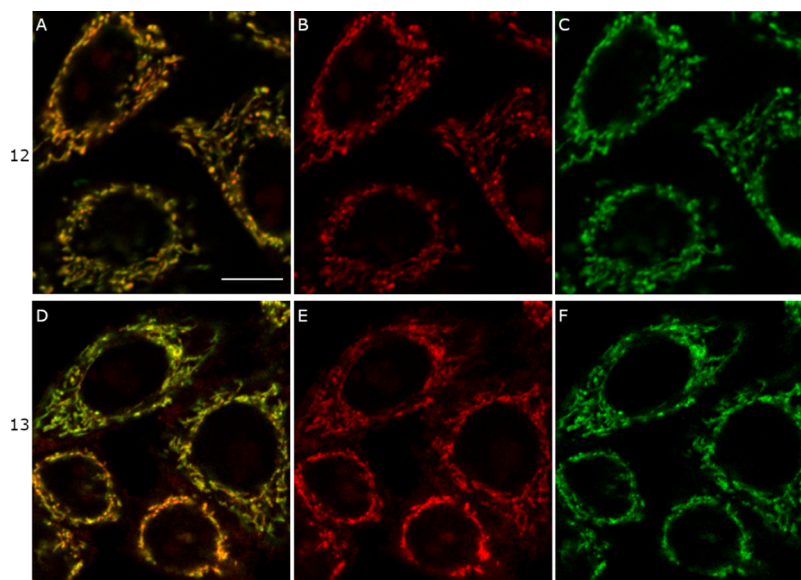


**Figure 5.** Colocalization studies with COUPY dyes 12 (top) and 13 (bottom) and MitoTracker Green FM. Single confocal plane of HeLa cells incubated with 12 or 13 ( $2\ \mu\text{M}$ , red) and MitoTracker Green FM ( $0.1\ \mu\text{M}$ , green). (A, D) Overlay of the two staining. (B, E) coumarin 12 and 13 signal, respectively. (C, F) MitoTracker Green FM signal. Scale bar:  $10\ \mu\text{m}$ . All images are at the same scale as (A).

pyrimidine-containing coumarins and MTG. On the other hand, the Manders' coefficients (which ranges from 0 to 1, determining the intensities of one channel colocalizing with the other) also confirmed that 12 and 13 were mainly placed in the mitochondria. The degree of colocalization of 12 over MTG ( $M_1$  coefficient) was 0.40, whereas that of MTG over 12 ( $M_2$

coefficient) was 0.73. These values indicate that there is more MTG signal colocalizing with 12 than 12 colocalizing with MTG. The localization of the coumarin probe in other organelles such as nucleoli and intracellular vesicles accounts for the differences in both Manders' coefficients. It is worth noting that smaller values for  $M_1$  (0.28) and  $M_2$  (0.68) were

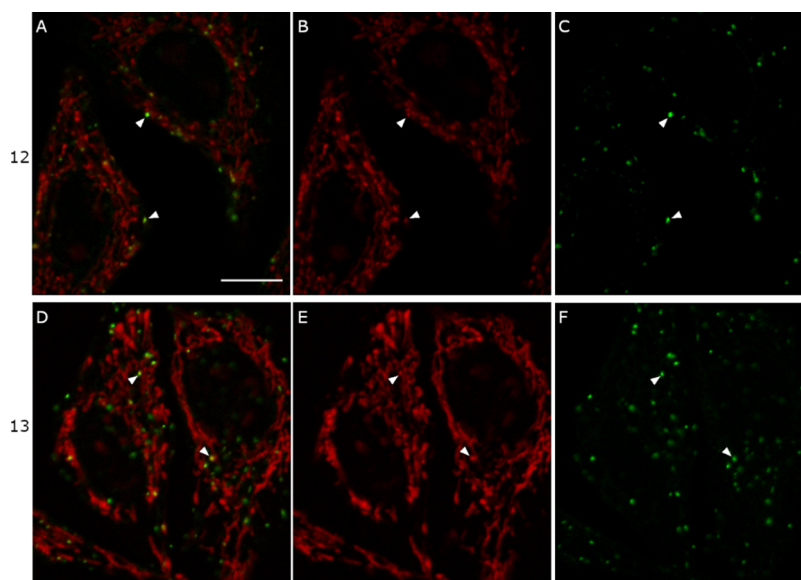


**Figure 6.** Colocalization studies with COUPY dyes and LysoTracker Green FM. Single confocal plane of HeLa cells incubated with coumarins **12** and **13** (2  $\mu$ M, red) and LysoTracker Green FM (0.2  $\mu$ M, green). (A, D) Overlay of the two staining. (B, E) coumarins **12** and **13** signal. (C, F) LysoTracker Green FM staining. White arrowheads point out COUPY dye vesicles colocalized with LysoTracker staining. Scale bar: 10  $\mu$ m. All images are at the same scale as (A).

obtained in the case of the parent coumarin **4**, which indicates that the signal from the fluorophore that colocalizes with MTG is higher in the case of pyrimidine-containing coumarin (**12**) than in the pyridine analogue (**4**), thereby suggesting a higher preference for mitochondria. Although not as pronounced, a similar trend was found for coumarins **13** ( $M_1 = 0.19$  and  $M_2 = 0.86$ ) and **5** ( $M_1 = 0.18$  and  $M_2 = 0.76$ ).

As previously observed with the parent fluorophores,<sup>12</sup> colocalization experiments with LTG (Figure 6) confirmed that most of the fluorescence observed in intracellular vesicles along the cytoplasm was associated with lysosome accumulation (Pearson's coefficients being equal to 0.52 (**12**) and 0.49 (**13**) on average). The smaller Mander's coefficients for the colocalization of the compounds over LTG ( $M_1 = 0.02$  for **12** and **13**) and of LTG over the coumarins ( $M_2 = 0.45$  for **12** and 0.62 for **13**) in the colocalization experiment with LTG compared with MTG might be explained by a reduced affinity of COUPY dyes for lysosome and/or by lower abundance of this organelle in cells compared with mitochondria.

Very interestingly, the nucleoli inside the nuclei was much less intensely stained in compounds **12** and **13** than in the parent coumarins: compare in Figure 4 panels (C) (**12**) and (D) (**13**) with panels (A) (**4**) and (B) (**5**), respectively. As shown in Figure 7, measurement of the mean fluorescence intensity both in the mitochondria and nucleoli confirmed this

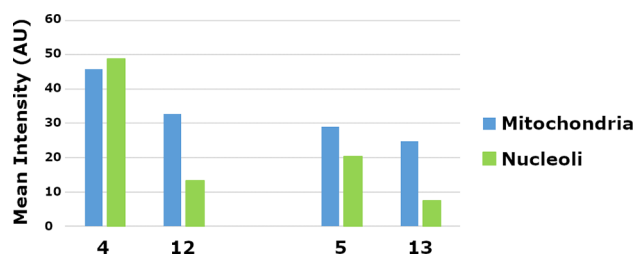


**Figure 7.** Graph of COUPY dyes **4**, **5**, **12**, and **13** vs mean intensity (Arbitrary Units) at the mitochondria and nucleoli.

observation. Indeed, the mean intensity for mitochondria and nucleoli was quite similar in the parent coumarins **4** and **5**, whereas the mean intensity for nucleoli staining was considerably reduced in case of the pyrimidine analogues **12** and **13**. These results are in line with the higher  $M_1$  coefficients measured in colocalization experiments with MTG and indicate that replacement of *para*-pyridine by *ortho,para*-pyrimidine in COUPY dyes caused an increase in the selectivity of the compounds toward mitochondria.

Finally, the photostability of coumarins **12** and **13** was evaluated in a more realistic situation and compared with that of the parent compounds (**4** and **5**, respectively). For this purpose, living HeLa cells were incubated at 37  $^{\circ}$ C with the compounds and irradiated continuously with the laser beam of the confocal microscope ( $\lambda_{\text{ex}} = 561$  nm at 4.32  $\mu$ W for **4** and **12**, and  $\lambda_{\text{ex}} = 633$  nm at 10.2  $\mu$ W for **5** and **13**) and images were acquired with an interval time of 0.42 s for 4.5 min. As shown in Figures S19 and S20, the overall fluorescence signal was significantly decreased in all the cases. In good agreement with the photobleaching studies (Figure 3), the *ortho,para*-containing coumarin **12** was found to be slightly more photostable than its parent compound (**4**), while this trend was found to be opposite in the case of the 4- $\text{CF}_3$ -containing compounds. Nevertheless, it is worth noting that the laser power used in the photobleaching experiments was much higher than the one used during the conventional observation (0.3 and 1.7  $\mu$ W with 561 and 633 nm lasers, respectively), which confirms a good photostability and applicability of these molecules for imaging living cells by using fluorescence microscopy.

## CONCLUSIONS

In summary, in this manuscript we have investigated how the photophysical properties and subcellular accumulation of coumarin-based COUPY fluorophores can be fine-tuned through replacement of the *para*-pyridine moiety with different heterocycles (*ortho*-pyridine and *ortho,ortho*- or *ortho,para*-pyrimidine), with the aim of establishing new SPFR. COUPY



dyes **10–13** were easily obtained from cheap, commercially available compounds in three linear synthetic steps, the reaction of thiocoumarins with suitable heteroarylacetonitrile derivatives followed by N-methylation of the pyridine or pyrimidine moieties being the key steps. Very interestingly, the photophysical properties of the new fluorophores were strongly influenced by these modifications. On the one hand, the replacement of the *para*-pyridine moiety with *ortho*-pyridine (**10**) or *ortho,ortho*-pyrimidine (**11**) had a negative effect on the spectroscopic properties of the dyes since both absorption and emission were blue-shifted, leading to weakly fluorescent compounds. On the other hand, the absorption and emission maxima of *ortho,para*-pyrimidine-containing fluorophores (**12–13**) were red-shifted with respect to the parent compounds, particularly in polar solvents. Besides emission in the far-red to NIR region, the newly synthesized fluorophores exhibited other appropriate characteristics for bioimaging applications such as large Stokes' shifts and high photostability. Furthermore, coumarins **12** and **13** retained the excellent cell permeability of COUPY dyes but exhibited a higher preference for mitochondria. Overall, these results provide useful indications for the development of novel mitochondria-targeted fluorescent probes based on small organic compounds since we have demonstrated that the selectivity for this organelle can be improved through the replacement of the N-alkylated pyridinium moieties by the corresponding N-alkylated *ortho,para*-pyrimidinium counterparts.

## ■ EXPERIMENTAL SECTION

**Materials and Methods.** Unless otherwise stated, common chemicals and solvents (HPLC grade or reagent grade quality) were purchased from commercial sources and used without further purification. Aluminum plates coated with a 0.2 mm-thick layer of silica gel 60 F<sub>254</sub> were used for thin-layer chromatography (TLC) analysis, whereas flash column chromatography purification was carried out using silica gel 60 (230–400 mesh). Reversed-phase HPLC analyses were carried out on a Jupiter Proteo C<sub>18</sub> column (250 × 4.6 mm, 90 Å 4 μm, flow rate: 1 mL/min) using linear gradients of 0.1% formic acid in H<sub>2</sub>O (A) and 0.1% formic acid in ACN (B). NMR spectra were recorded at 25 °C in a 400 MHz spectrometer using the deuterated solvent as an internal deuterium lock. The residual protic signal of chloroform or DMSO was used as a reference in <sup>1</sup>H and <sup>13</sup>C NMR spectra recorded in CDCl<sub>3</sub> or DMSO-*d*<sub>6</sub>, respectively. Chemical shifts are reported in parts per million (ppm) in the δ scale, coupling constants in Hz, and multiplicity as follows: s (singlet), d (doublet), t (triplet), q (quartet), qt (quintuplet), m (multiplet), dd (doublet of doublets), dq (doublet of quartets), br (broad signal), etc. The proton signals of the *E* and *Z* rotamers were identified by simple inspection of the <sup>1</sup>H spectrum and the rotamer ratio was calculated by peak integration. 2D-NOESY spectra were acquired in DMSO-*d*<sub>6</sub> with a mixing time of 500 ms, either at 298 K or 350 K. Electrospray ionization mass spectra (ESI-MS) were recorded on an instrument equipped with a single quadrupole detector coupled to an HPLC, and high-resolution (HR) ESI-MS on a LC/MS-TOF instrument.

**Synthesis of Pyrimidin-Acetonitrile Derivatives.** 2-(Pyrimidin-2-yl)acetonitrile (**15**). A solution of KCN (0.63 g, 9.70 mmol) in DMSO (5 mL) was slowly added to a solution of 2-(chloromethyl)-pyrimidine (0.5 g, 3.89 mmol) in DMSO (4 mL). The reaction mixture was stirred overnight at 35 °C with a hot plate magnetic stirrer. After addition of 50 mL of K<sub>2</sub>CO<sub>3</sub> (10%), the aqueous phase was extracted with diethyl ether (10 × 30 mL). The combined organic fractions were dried over anhydrous Na<sub>2</sub>SO<sub>4</sub>, filtered, and evaporated under reduced pressure. The crude product was purified by column chromatography (silica gel, 0–15% ethyl acetate in DCM) to give 84 mg of colorless oil (yield 19%). TLC: R<sub>f</sub> (ethyl acetate/DCM 1:1) 0.44. <sup>1</sup>H NMR (400 MHz, CDCl<sub>3</sub>, δ (ppm)): 8.74 (2H, d, J = 5.1

Hz), 7.29 (1H, t, J = 5.1 Hz), 4.11 (s, 2H). <sup>13</sup>C{<sup>1</sup>H} NMR (101 MHz, CDCl<sub>3</sub>, δ (ppm)): 161.4, 158.0, 120.3, 116.1, 28.6. LRMS (ESI-TOF) (*m/z*): [M + H]<sup>+</sup> Calcd for C<sub>6</sub>H<sub>6</sub>N<sub>3</sub>, 120.06; found, 119.90.

2-(Pyrimidin-4-yl)acetonitrile (**16**). A modified method was followed to synthesize compound **16**.<sup>19</sup>

(*E*)-*N,N*-Dimethyl-2-(pyrimidin-4-yl)ethen-1-amine (**17**). 4-Methylpyrimidine (10 g, 106 mmol) and 1,1-dimethoxy-*N,N*-dimethylmethanamine (38 g, 319 mmol) were dissolved in 50 mL of anhydrous DMF. The solution was heated at 140 °C with a hot plate magnetic stirrer for 24 h. The crude product was evaporated under reduced pressure to provide **17** as brown oil, which was used without further purification. TLC: R<sub>f</sub> (DCM/MeOH 9:1) 0.50. <sup>1</sup>H NMR (400 MHz, CDCl<sub>3</sub>, δ (ppm)): 8.73 (1H, s), 8.21 (1H, d, J = 5.6 Hz), 7.76 (1H, d, J = 13 Hz), 6.71 (1H, dd, J = 5.6, 1.6 Hz), 4.99 (1H, d, J = 13 Hz), 2.95 (6H, s).

2-(Pyrimidin-4-yl)acetonitrile (**16**). A solution of hydroxylamine-O-sulfonic acid (7.31 g, 57.5 mmol) in Milli-Q water (100 mL) was added to the crude product **17**, and the reaction mixture was heated at 50 °C with a hot plate magnetic stirrer for 45 min. Then, the mixture was cooled at 0 °C and saturated NaHCO<sub>3</sub> was added until basic pH, and the aqueous phase was extracted with ethyl acetate (6 × 200 mL). The combined organic phases were dried over anhydrous Na<sub>2</sub>SO<sub>4</sub>, filtered, and evaporated under reduced pressure. The brown oil was purified by column chromatography (silica gel, 0–25% ethyl acetate in DCM) to give 1.46 g of a yellow solid (yield 11%). TLC: R<sub>f</sub> (ethyl acetate/DCM 1:1) 0.34. <sup>1</sup>H NMR (400 MHz, CDCl<sub>3</sub>, δ (ppm)): 9.20 (1H, s), 8.80 (1H, d, J = 5.2 Hz), 7.51 (1H, d, J = 5.2 Hz), 3.94 (2H, s). <sup>13</sup>C{<sup>1</sup>H} NMR (101 MHz, CDCl<sub>3</sub>, δ (ppm)): 159.3, 159.2, 158.3, 119.7, 115.5, 26.5. LRMS (ESI-TOF) (*m/z*): [M + H]<sup>+</sup> Calcd for C<sub>6</sub>H<sub>6</sub>N<sub>3</sub>, 120.06; found, 119.90.

**Synthesis of COUPY Scaffolds (6–9).** 2-(Cyano(2-pyridine)methylene)-7-(*N,N*-diethylamino)-4-methyl-coumarin (**6**). 7-(*N,N*-Diethylamino)-4-methyl-2-thiocoumarin **18** (0.25 g, 1.01 mmol), 2-(pyridin-2-yl)acetonitrile **14** (0.24 g, 2.02 mmol), and NaH (60% dispersion in mineral oil, 0.36 g, 9 mmol) were dissolved in anhydrous acetonitrile (15 mL) and the mixture was stirred for 2 h under an argon atmosphere at room temperature and protected from light. Then, AgNO<sub>3</sub> (0.34 g, 2.02 mmol) was added and the resulting mixture was stirred for 2 h under Ar at room temperature. The crude product was evaporated under reduced pressure and purified by column chromatography (silica gel, 0–25% ethyl acetate in DCM) to give 240 mg of an orange solid (yield 72%). TLC: R<sub>f</sub> (ethyl acetate/DCM 1:1) 0.90. <sup>1</sup>H NMR (400 MHz, DMSO-*d*<sub>6</sub>, δ (ppm)): (*E* + *Z* rotamers) 8.56 (1H, m), 8.13 (0.6H, dt, J = 8.2, 0.8 Hz), 7.82 (1.4H, m), 7.46 (1.4H, m), 7.18 (1H, m), 6.70 (1H, dd, J = 9.0, 2.4 Hz), 6.65 (1.2H, m), 6.42 (0.4H, d, J = 2.4 Hz), 3.46 (4H, q, J = 7.2 Hz), 2.35 (1.8H, d, J = 0.8 Hz), 2.32 (1.2H, d, J = 0.8 Hz), 1.14 (6H, m). <sup>13</sup>C{<sup>1</sup>H} NMR (101 MHz, DMSO-*d*<sub>6</sub>, δ (ppm)): (*E* + *Z* rotamers) 163.2, 161.8, 154.0, 153.8, 152.7, 152.0, 150.6, 150.5, 149.0, 148.8, 144.6, 144.0, 137.1, 136.8, 126.0, 125.9, 121.8, 121.2, 120.7, 120.2, 119.6, 119.3, 110.8, 110.4, 109.8, 109.2, 109.1, 96.7, 96.1, 85.3, 81.0, 44.0, 43.8, 18.5, 18.0, 12.4. HRMS (ESI-TOF) (*m/z*): [M + H]<sup>+</sup> Calcd for C<sub>21</sub>H<sub>22</sub>N<sub>3</sub>O, 332.1763; found, 332.1759. Analytical HPLC (30–100% B in 30 min, formic acid additive): R<sub>t</sub> = 15.2 min.

2-(Cyano(2-pyrimidine)methylene)-7-(*N,N*-diethylamino)-4-methyl-coumarin (**7**). 7-(*N,N*-Diethylamino)-4-methyl-2-thiocoumarin **18** (0.25 g, 1.01 mmol), 2-(pyrimidin-2-yl)acetonitrile **15** (0.24 g, 2.02 mmol), and NaH (60% dispersion in mineral oil, 0.36 g, 9 mmol) were dissolved in anhydrous acetonitrile (15 mL) and the mixture was stirred for 2 h under an argon atmosphere at room temperature and protected from light. Then, AgNO<sub>3</sub> (0.34 g, 2.02 mmol) was added and the resulting mixture was stirred for 2 h under Ar at room temperature. The crude product was evaporated under reduced pressure and purified by column chromatography (silica gel, 0–10% ethyl acetate in DCM) to give 171 mg of an orange solid (yield 51%). TLC: R<sub>f</sub> (ethyl acetate/DCM 1:1) 0.63. <sup>1</sup>H NMR (400 MHz, DMSO-*d*<sub>6</sub>, δ (ppm)): (major rotamer) 8.74 (2H, d, J = 4.8 Hz), 8.18 (1H, s), 7.53 (1H, d, J = 9.0 Hz), 7.17 (1H, t, J = 4.8 Hz), 6.76 (1H, dd, J = 9.0, 2.4 Hz), 6.46 (1H, d, J = 2.4 Hz), 3.47 (4H, q, J = 7.2 Hz), 2.39 (3H, s), 1.15 (6H, t, J = 6.9 Hz). <sup>13</sup>C{<sup>1</sup>H} NMR (101



MHz, DMSO- $d_6$ ,  $\delta$  (ppm)): (major rotamer) 166.6, 162.9, 157.0, 154.1, 150.9, 146.6, 126.3, 118.4, 116.6, 110.5, 109.9, 109.7, 96.0, 82.5, 44.1, 18.7, 12.4. HRMS (ESI-TOF) ( $m/z$ ):  $[M + H]^+$  Calcd for  $C_{20}H_{21}N_4O$ , 333.1715; found, 333.1710. Analytical HPLC (30–100% B in 30 min, formic acid additive):  $R_t$  = 21.2 min.

**2-(Cyano(4-pyrimidine)methylene)-7-(*N,N*-diethylamino)-4-methyl-coumarin (8).** 7-(*N,N*-Diethylamino)-4-methyl-2-thiocoumarin **18** (0.25 g, 1.01 mmol), 2-(pyrimidin-4-yl)acetonitrile **16** (0.24 g, 2.02 mmol), and NaH (60% dispersion in mineral oil, 0.36 g, 9 mmol) were dissolved in anhydrous acetonitrile (15 mL) and the mixture was stirred for 2 h under an argon atmosphere at room temperature and protected from light. Then,  $AgNO_3$  (0.34 g, 2.02 mmol) was added and the resulting mixture was stirred for 2 h under Ar at room temperature. The crude product was evaporated under reduced pressure and purified by column chromatography (silica gel, 0–25% ethyl acetate in DCM) to give 275 mg of an orange solid (yield 82%). TLC:  $R_f$  (ethyl acetate/DCM 1:1) 0.50.  $^1H$  NMR (400 MHz, DMSO- $d_6$ ,  $\delta$  (ppm)): (E + Z rotamers) 9.04 (1H, m), 8.69 (0.6H, d,  $J$  = 5.6 Hz), 8.62 (0.4H, d,  $J$  = 5.6 Hz), 8.26 (0.4H, d,  $J$  = 0.8 Hz), 8.18 (0.6H, dd,  $J$  = 5.6, 1.6 Hz), 7.59 (0.4H, d,  $J$  = 9.2 Hz), 7.56 (0.6H, d,  $J$  = 8.8 Hz), 7.42 (0.4H, dd,  $J$  = 5.6, 1.6 Hz), 6.81 (1.6H, m), 6.75 (0.6H, d,  $J$  = 0.8 Hz), 6.51 (0.4H, d,  $J$  = 2.8 Hz), 3.49 (4H, m), 2.43 (1.2H, d,  $J$  = 1.2 Hz), 2.42 (1.7H, d,  $J$  = 1.2 Hz), 1.16 (6H, t,  $J$  = 7.0 Hz).  $^{13}C\{^1H\}$  NMR (101 MHz, DMSO- $d_6$ ,  $\delta$  (ppm)): (E + Z rotamers) 165.5, 165.2, 160.3, 159.1, 158.1, 157.6, 156.9, 156.7, 154.2, 151.2, 151.0, 148.5, 147.6, 126.5, 126.4, 118.6, 118.4, 117.5, 116.9, 116.7, 110.6, 110.4, 110.3, 110.2, 109.2, 96.6, 95.8, 82.8, 78.5, 44.1, 43.9, 18.8, 18.2, 12.4, 12.3. HRMS (ESI-TOF) ( $m/z$ ):  $[M + H]^+$  Calcd for  $C_{20}H_{21}N_4O$ , 333.1715; found, 333.1709. Analytical HPLC (30–100% B in 30 min, formic acid additive):  $R_t$  = 17.5 min.

**2-(Cyano(4-pyrimidine)methylene)-7-(*N,N*-dimethylamino)-4-trifluoromethyl-coumarin (9).** 7-(*N,N*-Dimethylamino)-4-trifluoromethyl-2-thiocoumarin **19** (0.25 g, 0.92 mmol), 2-(pyrimidin-4-yl)acetonitrile **16** (0.22 g, 1.83 mmol), and NaH (60% dispersion in mineral oil, 0.33 g, 8.25 mmol) were dissolved in anhydrous acetonitrile (15 mL) and the mixture was stirred for 2 h under an argon atmosphere at room temperature and protected from light. Then,  $AgNO_3$  (0.31 g, 1.83 mmol) was added and the resulting mixture was stirred for 2 h under Ar at room temperature. The crude product was evaporated under reduced pressure and purified by column chromatography (silica gel, 0–10% ethyl acetate in DCM) to give 248 mg of a red solid (yield 75%). TLC:  $R_f$  (ethyl acetate/DCM 1:1) 0.30 and 0.64.  $^1H$  NMR (400 MHz, DMSO- $d_6$ ,  $\delta$  (ppm)): (E + Z rotamers) 9.17 (0.55H, d,  $J$  = 1.2 Hz), 9.15 (0.45H, d,  $J$  = 1.2 Hz), 8.83 (0.55H, d,  $J$  = 5.6 Hz), 8.78 (0.45H, d,  $J$  = 5.6 Hz), 8.74 (0.45H, s), 8.28 (0.55H, dd,  $J$  = 5.6, 1.6 Hz), 7.56 (0.45H, dd,  $J$  = 5.6, 1.6 Hz), 7.44 (1H, m), 7.03 (0.55H, s), 7.00 (0.55H, d,  $J$  = 2.8 Hz), 6.87 (1H, m), 6.64 (0.45H, d,  $J$  = 2.4 Hz), 3.13 (3.3H, s), 3.11 (2.7H, s).  $^{13}C\{^1H\}$  NMR (101 MHz, DMSO- $d_6$ ,  $\delta$  (ppm)): (E + Z rotamers) 163.3, 162.6, 158.7, 158.3, 157.9, 157.7, 157.6, 154.6, 154.5, 153.7, 153.6, 125.3, 118.8, 117.9, 117.4, 116.8, 111.0, 110.9, 110.8, 110.7, 110.7, 110.5, 110.4, 110.4, 103.5, 102.5, 98.1, 97.4, 89.7, 89.5, 85.2, 39.7.  $^{19}F$  NMR (376 MHz, DMSO- $d_6$ ,  $\delta$  (ppm)): (E + Z rotamers) –63.0 (1.35F, s), –63.1 (1.65F, s). HRMS (ESI-TOF) ( $m/z$ ):  $[M + H]^+$  Calcd for  $C_{18}H_{14}F_3N_4O$ , 359.1114; found, 359.1112. Analytical HPLC (30–100% B in 30 min, formic acid additive):  $R_t$  = 22.8 min.

**Synthesis of COUPY Fluorophores (10–13).** **2-(Cyano(1-methyl(2-pyridin-1-ium))methylene)-7-(*N,N*-diethylamino)-4-methyl-coumarin triflate (10).** Methyl trifluoromethanesulfonate (47.5  $\mu$ L, 0.42 mmol) was added to a solution of 2-(cyano(2-pyridine)methylene)-7-(*N,N*-diethylamino)-4-methyl-coumarin **6** (70 mg, 0.21 mmol) in DCM (30 mL) under an argon atmosphere. The mixture was stirred for 4 h at room temperature and protected from light. The reaction mixture was evaporated under reduced pressure and purified by column chromatography (silica gel, 0–3% MeOH in DCM) to give 77 mg of a red solid (yield 74%). TLC:  $R_f$  (DCM/MeOH 9:1) 0.35.  $^1H$  NMR (400 MHz, 77  $^{\circ}C$ , DMSO- $d_6$ ,  $\delta$  (ppm)): 9.02 (1H, d,  $J$  = 6.4 Hz), 8.53 (1H, td,  $J$  = 7.6, 1.2 Hz), 8.26 (1H, d,  $J$  = 8.0 Hz), 8.00 (1H, td,  $J$  = 7.6, 1.2 Hz), 7.59 (1H, d,  $J$  = 9.2 Hz), 6.83 (1H, dd,  $J$  = 9.2, 2.4 Hz), 6.62 (1H, br s), 6.51 (1H, br s), 4.28

(3H, s), 3.46 (4H, q,  $J$  = 7.2 Hz), 2.43 (3H, s), 1.15 (6H, t,  $J$  = 7.2 Hz).  $^{13}C\{^1H\}$  NMR (101 MHz, 77  $^{\circ}C$ , DMSO- $d_6$ ,  $\delta$  (ppm)): 165.6, 153.9, 151.2, 149.3, 147.8, 147.1, 144.6, 130.5, 126.2, 125.3, 120.5 (q,  $J$  = 323 Hz,  $T_f$ ), 116.5, 110.3, 109.4, 108.0, 96.2, 71.0, 46.0, 43.7, 17.6, 12.0.  $^{19}F$  NMR (376 MHz, DMSO- $d_6$ ,  $\delta$  (ppm)): –77.8 (3F, s). HRMS (ESI-TOF) ( $m/z$ ):  $[M]^+$  Calcd for  $C_{22}H_{24}N_3O$ , 346.1914; found, 346.1911. Analytical HPLC (30–100% B in 30 min, formic acid additive):  $R_t$  = 5.5 min.

**2-(Cyano(1-methyl(2-pyrimidin-1-ium))methylene)-7-(*N,N*-diethylamino)-4-methyl-coumarin triflate (11).** Methyl trifluoromethanesulfonate (47.5  $\mu$ L, 0.42 mmol) was added to a solution of 2-(cyano(2-pyrimidine)methylene)-7-(*N,N*-diethylamino)-4-methyl-coumarin **7** (70 mg, 0.21 mmol) in DCM (30 mL) under an argon atmosphere. The mixture was stirred for 4 h at room temperature and protected from light. Then, an additional amount of methyl trifluoromethanesulfonate (47.5  $\mu$ L, 0.42 mmol) was added to the reaction mixture and was stirred for 2 h. The reaction mixture was evaporated under reduced pressure and purified by column chromatography (silica gel, 0–4% MeOH in DCM) to give 66 mg of an orange solid (yield 64%). TLC:  $R_f$  (DCM/MeOH 9:1) 0.31.  $^1H$  NMR (400 MHz, DMSO- $d_6$ ,  $\delta$  (ppm)): 9.28 (1H, dd,  $J$  = 4.2, 2.0 Hz), 9.16 (1H, dd,  $J$  = 6.6, 1.8 Hz), 7.91 (1H, dd,  $J$  = 6.4, 5.6 Hz, 1H), 7.70 (1H, d,  $J$  = 9.2 Hz), 7.06 (1H, s), 6.94 (1H, dd,  $J$  = 9.2, 2.8 Hz), 6.70 (1H, d,  $J$  = 2.8 Hz), 4.14 (3H, s), 3.50 (4H, q,  $J$  = 7.2 Hz), 2.49 (3H, s), 1.15 (6H, t,  $J$  = 7.2 Hz).  $^{13}C\{^1H\}$  NMR (101 MHz, DMSO- $d_6$ ,  $\delta$  (ppm)): 162.9157.6, 154.7, 154.6, 152.5, 151.8, 127.1, 120.7 (q,  $J$  = 323 Hz,  $T_f$ ), 118.7, 116.8, 111.6, 110.4, 109.2, 96.0, 73.4, 46.5, 44.2, 18.5, 12.3.  $^{19}F$  NMR (376 MHz, DMSO- $d_6$ ,  $\delta$  (ppm)): –77.8 (3F, s). HRMS (ESI-TOF) ( $m/z$ ):  $[M]^+$  Calcd for  $C_{21}H_{23}N_4O$ , 347.1866; found, 347.1865. Analytical HPLC (30–100% B in 30 min, formic acid additive):  $R_t$  = 5.1 min.

**2-(Cyano(1-methyl(4-pyrimidin-1-ium))methylene)-7-(*N,N*-diethylamino)-4-methyl-coumarin triflate (12).** Methyl trifluoromethanesulfonate (47.5  $\mu$ L, 0.42 mmol) was added to a solution of 2-(cyano(4-pyrimidine)methylene)-7-(*N,N*-diethylamino)-4-methyl-coumarin **8** (70 mg, 0.21 mmol) in DCM (30 mL) under an argon atmosphere. The mixture was stirred for 4 h at room temperature and protected from light. The reaction mixture was evaporated under reduced pressure and purified by column chromatography (silica gel, 0–2% MeOH in DCM) to give 83 mg of a violet solid (yield 80%). TLC:  $R_f$  (DCM/MeOH 9:1) 0.28.  $^1H$  NMR (400 MHz, 77  $^{\circ}C$ , DMSO- $d_6$ ,  $\delta$  (ppm)): 9.11 (1H, m), 8.53 (1H, dd,  $J$  = 7.6, 2.0 Hz), 8.00 (1H, d,  $J$  = 7.6 Hz), 7.84 (1H, d,  $J$  = 9.2 Hz), 7.60 (1H, br s), 7.09 (1H, dd,  $J$  = 9.2, 2.4 Hz), 6.89 (1H, d,  $J$  = 2.4 Hz), 4.02 (3H, s), 3.60 (4H, q,  $J$  = 7.2 Hz), 2.63 (3H, s), 1.23 (6H, t,  $J$  = 7.2 Hz).  $^{13}C\{^1H\}$  NMR (101 MHz, DMSO- $d_6$ ,  $\delta$  (ppm)): 167.3, 163.4, 155.6, 155.5, 152.7, 152.2, 147.5, 127.5, 120.7 (q,  $J$  = 323 Hz,  $T_f$ ), 117.4, 114.8, 113.1, 111.5, 110.7, 95.9, 44.4, 42.5, 18.9, 12.4.  $^{19}F$  NMR (376 MHz, DMSO- $d_6$ ,  $\delta$  (ppm)): –77.8 (3F, s). HRMS (ESI-TOF) ( $m/z$ ):  $[M]^+$  Calcd for  $C_{21}H_{23}N_4O$ , 347.1866; found, 347.1866. Analytical HPLC (30–100% B in 30 min, formic acid additive):  $R_t$  = 5.4 min.

**2-(Cyano(1-methyl(4-pyrimidin-1-ium))methylene)-7-(*N,N*-dimethylamino)-4-trifluoromethyl-coumarin triflate (13).** Methyl trifluoromethanesulfonate (47.3  $\mu$ L, 0.40 mmol) was added to a solution of 2-(cyano(4-pyrimidine)methylene)-7-(*N,N*-dimethylamino)-4-trifluoromethyl-coumarin **9** (70 mg, 0.20 mmol) in DCM (30 mL) under an argon atmosphere. The mixture was stirred for 4 h at room temperature and protected from light. The reaction mixture was evaporated under reduced pressure and purified by column chromatography (silica gel, 0–2% MeOH in DCM) to give 75 mg of a blue solid (yield 72%). TLC:  $R_f$  (DCM/MeOH 9:1) 0.48.  $^1H$  NMR (400 MHz, 77  $^{\circ}C$ , DMSO- $d_6$ ,  $\delta$  (ppm)): 9.40 (1H, s), 8.81 (1H, dd,  $J$  = 7.4, 1.8 Hz), 8.21 (1H, br s), 7.65 (1H, dq,  $J$  = 9.2, 2.0 Hz), 7.13 (1H, dd,  $J$  = 9.2, 2.6 Hz), 7.01 (1H, br s), 4.13 (3H, s), 3.22 (6H, s).  $^{13}C\{^1H\}$  NMR (101 MHz, 77  $^{\circ}C$ , DMSO- $d_6$ ,  $\delta$  (ppm)): 166.8, 163.2, 158.8, 156.0, 155.4, 154.5, 153.1, 152.4, 136.7 (q,  $J$  = 32 Hz), 125.4, 124.9, 121.5 (q,  $J$  = 277 Hz), 120.5 (q,  $J$  = 323 Hz), 116.6, 115.6, 113.3, 109.7, 108.4, 107.7, 101.5, 97.7, 97.2, 43.0, 40.0.  $^{19}F$  NMR (376 MHz, DMSO- $d_6$ ,  $\delta$  (ppm)): –63.1 (3F, s), –77.8 (3F, s). HRMS (ESI-TOF) ( $m/z$ ):  $[M]^+$  Calcd for  $C_{19}H_{16}F_3N_4O$ , 373.1271;

found, 373.1274. Analytical HPLC (30–100% B in 30 min, formic acid additive):  $R_t = 5.1$  min.

**Photophysical Characterization of the Compounds.** Absorption spectra were recorded on a Jasco V-730 spectrophotometer at room temperature. Molar absorption coefficients ( $\epsilon$ ) were determined by direct application of the Beer–Lambert law, using solutions of the compounds in each solvent with concentrations ranging from  $10^{-6}$  to  $10^{-5}$  M. Emission spectra were measured on a Photon Technology International (PTI) fluorimeter. Fluorescence quantum yields ( $\Phi_F$ ) were measured by a comparative method using Cresyl Violet in ethanol ( $\Phi_{F,Ref} = 0.54$ ) as a reference for compounds **4**, **5**, **12**, and **13**. Fluorescein dissolved in aqueous sodium hydroxide (0.1 M;  $\Phi_{F,Ref} = 0.92$ ) was used as a reference in the case of compounds **10** and **11**.<sup>17</sup> Then, optically matched solutions of the compounds and CV were prepared and fluorescence spectra were recorded. The absorbance of the sample and reference solutions was set below 0.1 at the excitation wavelength and  $\Phi_F$  was calculated using the following eq 1:

$$\Phi_{F,Sample} = \frac{Area_{Sample}}{Area_{Ref}} \times \left( \frac{\eta_{Sample}}{\eta_{Ref}} \right)^2 \times \Phi_{F,ref} \quad (1)$$

where  $Area_{Sample}$  and  $Area_{Ref}$  are the integrated fluorescence for the sample and the reference and  $\eta_{Sample}$  and  $\eta_{Ref}$  are the refractive index of the sample and reference solutions, respectively. The uncertainty in the experimental value of  $\Phi_F$  has been estimated to be approximately 10%.

Photostability studies were performed by monitoring fluorescence bleaching of a 5  $\mu$ M PBS solution (pH 7.4) of the compounds at 37 °C irradiated with a high power 505 nm LED (100 mW/cm<sup>2</sup>). Fluorescence intensity values were recorded at  $t = 0$  ( $F_0$ ) and after different irradiation times ( $F$ ).

**Cell Culture and Treatments.** HeLa cells were maintained in DMEM (Dulbecco's Modified Eagle Medium) containing high glucose (4.5 g/L) and supplemented with 10% fetal calf serum (FCS) and 50 U/mL penicillin–streptomycin. For cellular uptake experiments and posterior observation under a microscope, cells were seeded on glass-bottom dishes (P35G-1.5-14-C, Mattek). The cells were incubated for 30 min at 37 °C with COUPY dyes (**4**, **5**, **12**, or **13**, 2  $\mu$ M) in supplemented DMEM, 24 hours after cell seeding. Then, the cells were washed three times with DPBS (Dulbecco's phosphate buffered saline, pH 7.0–7.3) to remove the excess fluorophores and kept in low glucose DMEM without phenol red for fluorescence imaging.

For colocalization experiments with MitoTracker Green FM, HeLa cells were treated with COUPY dyes (2  $\mu$ M) and MitoTracker Green FM (0.1  $\mu$ M) for 30 min at 37 °C in nonsupplemented DMEM. After removal of the medium and washing three times with DPBS, cells were kept in low glucose DMEM without phenol red for fluorescence imaging.

For colocalization experiments with LysoTracker Green FM and Hoechst 33342, HeLa cells were treated with COUPY dyes (2  $\mu$ M) and LysoTracker Green FM (0.2  $\mu$ M) for 30 min at 37 °C in nonsupplemented DMEM. After removal of the medium and washing three times with DPBS, the cells were incubated for 10 min at 37 °C with Hoechst 33342 (1  $\mu$ g/mL) in supplemented DMEM. Finally, the cells were washed and kept in low glucose DMEM without phenol red for fluorescence imaging.

**Fluorescence Imaging.** All microscopy observations were performed using a Zeiss LSM 880 confocal microscope equipped with a 405 nm laser diode, an argon-ion laser, a 561 nm laser, and a 633 nm laser. The microscope was also equipped with a Heating Insert P S (Pecon) and a 5% CO<sub>2</sub> providing system. Cells were observed at 37 °C using a 63  $\times$  1.2 glycerol immersion objective. Coumarins **4** and **12** were excited using the 561 nm laser and detected from 570 to 670 nm. Coumarins **5** and **13** were excited using the 633 nm laser and detected from 643 to 758 nm. In colocalization studies, MitoTracker Green FM and LysoTracker Green were observed using the 488 nm laser line of the argon-ion laser, whereas the 405 nm laser diode was used for observing Hoechst 33342.

Bleaching experiments were performed at 37 °C by continuous image acquisition with an interval time of 0.42 s for 4.5 min. Coumarins **4** and **12** were bleached using the 561 nm laser at 4.32  $\mu$ W and coumarins **5** and **13** were bleached with the 633 nm laser at 10.2  $\mu$ W.

Image processing and analysis was performed using Fiji.<sup>20</sup>

**Intensity Measurement.** The nuclei and coumarin channels were processed by median filtering (radius = 2), Gaussian filtering (sigma = 2), and background subtraction (rolling ball radius = 300). The mean intensity in the nucleoli was measured in the maximum intensity projection of the processed coumarin image after manually drawing ROIs around each nucleoli. The intensity measurement in mitochondria needed further processing. First, the nuclei were segmented using the Intermodes algorithm,<sup>21</sup> and the resulting binary image was processed by filling holes and opening operations. Then the binary image of the nuclei was subtracted to the processed coumarin image to get rid of any nuclear signal. After the subtraction, the coumarin staining channel was projected with the maximum intensity and the mitochondria were segmented using the Phansalkar algorithm (radius = 5).<sup>22</sup> The binary image of the mitochondria was used as a mask to obtain the coumarin signal in the mitochondria and then measure its mean intensity.

**Bleaching Analysis.** Images were first processed by median filtering (radius = 1) and background subtraction (rolling ball radius = 50). Then, an ROI was manually drawn around each cell and in the background to measure the mean intensity along time. Intensity normalization was performed using the following eq 2:

$$\text{Normalized intensity} = \frac{\text{Cell}(t) - \text{Backg}(t)}{\text{Cell}(0) - \text{Backg}(0)} \quad (2)$$

where  $\text{Cell}(t)$  is the mean intensity in a cell at  $t$  time,  $\text{Cell}(0)$  is the mean intensity in that cell at the beginning of the experiment,  $\text{Backg}(t)$  is the mean intensity in the background at  $t$  time, and  $\text{Backg}(0)$  is the mean intensity in the background at the beginning of the experiment. After intensity normalization, the time at which the intensity dropped to half the initial one ( $t_{50}$ ) was obtained. Differences between the different  $t_{50}$  of coumarin **4** and **12** were tested with Student's  $t$ -test.

**Colocalizations Coefficients.** The MitoTracker or LysoTracker and coumarin channels were processed by median filtering (radius = 1), Gaussian filtering (sigma = 1), and background subtraction (rolling ball radius = 300). Colocalization coefficients were measured using the JaCoP plugin<sup>17</sup> on the different stacks of images ( $n = 4$ ) with each stack containing 3–5 cells. The threshold for the coumarin channel was set to include the signal in the mitochondria, nucleoli, and vesicles. The threshold for the MitoTracker or LysoTracker channels was set to specifically select mitochondria and lysosomes, respectively.

## ■ ASSOCIATED CONTENT

### Supporting Information

The Supporting Information is available free of charge at <https://pubs.acs.org/doi/10.1021/acs.joc.0c00570>.

Copies of HPLC traces and UV–vis absorption and fluorescence emission spectra of the compounds; additional fluorescence imaging studies; and 1D NMR (<sup>1</sup>H, <sup>13</sup>C, and <sup>19</sup>F), MS, and selected 2D NMR spectra (PDF).

## ■ AUTHOR INFORMATION

### Corresponding Author

Vicente Marchán – Departament de Química Inorgànica i Orgànica, Secció de Química Orgànica, IBUB, Universitat de Barcelona, E-08028 Barcelona, Spain; [orcid.org/0000-0002-1905-2156](https://orcid.org/0000-0002-1905-2156); Email: [vmarchan@ub.edu](mailto:vmarchan@ub.edu)

## Authors

**Anna Rovira** – Departament de Química Inorgànica i Orgànica, Secció de Química Orgànica, IBUB, Universitat de Barcelona, E-08028 Barcelona, Spain

**Miriam Pujals** – Departament de Química Inorgànica i Orgànica, Secció de Química Orgànica, IBUB, Universitat de Barcelona, E-08028 Barcelona, Spain

**Albert Gandioso** – Departament de Química Inorgànica i Orgànica, Secció de Química Orgànica, IBUB, Universitat de Barcelona, E-08028 Barcelona, Spain

**Marta López-Corrales** – Departament de Química Inorgànica i Orgànica, Secció de Química Orgànica, IBUB, Universitat de Barcelona, E-08028 Barcelona, Spain

**Manel Bosch** – Unitat de Microscòpia Òptica Avançada, Centres Científics i Tecnològics, Universitat de Barcelona, E-08028 Barcelona, Spain

Complete contact information is available at:

<https://pubs.acs.org/10.1021/acs.joc.0c00570>

## Notes

The authors declare no competing financial interest.

## ACKNOWLEDGMENTS

This work was supported by funds from the Spanish Government (MCIU/AEI/FEDER, UE; grant CTQ2017-84779-R) and the Generalitat de Catalunya (2017 DI 072). The authors acknowledge the helpful assistance of Dr. Francisco Cárdenas (NMR) and Dr. Irene Fernández and Laura Ortiz (MS) from CCIUB. A.R. and A.G. were recipient fellows of the University of Barcelona.

## REFERENCES

- (1) (a) Lavis, L. D.; Raines, R. T. Bright Ideas for Chemical Biology. *ACS Chem. Biol.* **2008**, *3*, 142–155. (b) Yuan, L.; Lin, W.; Zheng, K.; He, L.; Huang, W. Far-red to near infrared analyte-responsive fluorescent probes based on organic fluorophore platforms for fluorescence imaging. *Chem. Soc. Rev.* **2013**, *42*, 622–661. (c) Lavis, L. D.; Raines, R. T. Bright Building Blocks for Chemical Biology. *ACS Chem. Biol.* **2014**, *9*, 855–866. (d) Zheng, Q.; Jüette, M. F.; Jockusch, S.; Wasserman, M. R.; Zhou, Z.; Altman, R. B.; Blanchard, S. C. Ultra-stable Organic Fluorophores for Single-molecule Research. *Chem. Soc. Rev.* **2014**, *43*, 1044–1056. (e) Zheng, Q.; Lavis, L. D. Development of photostable fluorophores for molecular imaging. *Curr. Opin. Chem. Biol.* **2017**, *39*, 32–38. (f) Freidus, L. G.; Pradeep, P.; Kumar, P.; Choonara, Y. E.; Pillay, V. Alternative Fluorophores Designed for Advanced Molecular Imaging. *Drug Discovery Today* **2018**, *23*, 115–133.
- (2) (a) Srinivasarao, M.; Galliford, C. V.; Low, P. S. Principles in the design of ligand-targeted cancer therapeutics and imaging agents. *Nat. Rev. Drug Discov.* **2015**, *14*, 203–219. (b) Zhang, R. R.; Schroeder, A. B.; Grudzinski, J. J.; Rosenthal, E. L.; Warram, J. M.; Pinchuk, A. N.; Eliceiri, K. W.; Kuo, J. S.; Weichert, J. P. Beyond the margins: realtime detection of cancer using targeted fluorophores. *Nat. Rev. Clin. Oncol.* **2017**, *14*, 347–364. (c) Gao, M.; Yu, F.; Lv, C.; Choo, J.; Chen, L. Fluorescent chemical probes for accurate tumor diagnosis and targeting therapy. *Chem. Soc. Rev.* **2017**, *46*, 2237–2271.
- (3) Alamudi, S. H.; Chang, Y.-T. Advances in the design of cell-permeable fluorescent probes for applications in live cell imaging. *Chem. Commun.* **2018**, *54*, 13641–13653.
- (4) Apostolova, N.; Blas-García, A.; Esplugues, J. V. Mitochondria sentencing about cellular life and death: a matter of oxidative stress. *Curr. Pharm. Des.* **2011**, *17*, 4047–4060.
- (5) (a) Modica-Napolitano, J. S.; Singh, K. K. Mitochondrial dysfunction in cancer. *Mitochondrion* **2004**, *4*, 755–762. (b) Lin, M. T.; Beal, M. F. Mitochondrial dysfunction and oxidative stress in neurodegenerative diseases. *Nature* **2006**, *443*, 787–795. (c) Sun, N.; Youle, R. J.; Finkel, T. The Mitochondrial Basis of Aging. *Mol. Cell* **2016**, *61*, 654–666. (d) Hou, X.-S.; Wang, H.-S.; Mugaka, B. P.; Yang, G.-J.; Ding, Y. Mitochondria: promising organelle targets for cancer diagnosis and treatment. *Biomater. Sci.* **2018**, *6*, 2786–2797.
- (6) Hu, F.; Cai, X.; Manghnani, P. N.; Kenry, K.; Wu, W.; Liu, B. Multicolor monitoring of cellular organelles by single wavelength excitation to visualize the mitophagy process. *Chem. Sci.* **2018**, *9*, 2756–2761.
- (7) (a) Wang, Y.; Liu, T.; Zhang, E.; Luo, S.; Tan, X.; Shi, C. Preferential accumulation of the near infrared heptamethine dye IR-780 in the mitochondria of drug-resistant lung cancer cells. *Biomaterials* **2014**, *35*, 4116–4124. (b) Yang, X.; Shi, C.; Tong, R.; Qian, W.; Zhau, H. E.; Wang, R.; Zhu, G.; Cheng, J.; Yang, V. W.; Cheng, T.; Henary, M.; Strekowski, L.; Chung, L. W. K. Near IR Heptamethine Cyanine Dye-Mediated Cancer Imaging. *Clin. Cancer Res.* **2010**, *16*, 2833–2844. (c) Johnson, L. V.; Walsh, M. L.; Chen, L. B. Localization of mitochondria in living cells with rhodamine 123. *Proc. Natl. Acad. Sci. U. S. A.* **1980**, *77*, 990–994.
- (8) (a) Zhang, W.; Kwok, R. T. K.; Chen, Y.; Chen, S.; Zhao, E.; Yu, C. Y. Y.; Lam, J. W. Y.; Zheng, Q.; Tang, B. Z. Real-time monitoring of the mitophagy process by a photostable fluorescent mitochondrion-specific bioprobe with AIE characteristics. *Chem. Commun.* **2015**, *51*, 9022–9025. (b) Xu, W.; Zeng, Z.; Jiang, J.-H.; Chang, Y.-T.; Yuan, L. Discerning the Chemistry in Individual Organelles with Small-Molecule Fluorescent Probes. *Angew. Chem. Int. Ed.* **2016**, *55*, 13658–13699. (c) Sung, J.; Lee, Y.; Cha, J.-H.; Park, S. B.; Kim, E. Development of fluorescent mitochondria probe based on 1,2-dihydropyrrolo[3,4-b]indolizine-3-one. *Dyes Pigm.* **2017**, *145*, 461–468. (d) Zielonka, J.; Joseph, J.; Sikora, A.; Hardy, M.; Ouari, O.; Vasquez-Vivar, J.; Cheng, G.; Lopez, M.; Kalyanaraman, B. Mitochondria-Targeted Triphenylphosphonium-Based Compounds: Syntheses, Mechanisms of Action, and Therapeutic and Diagnostic Applications. *Chem. Rev.* **2017**, *117*, 10043–10120.
- (9) (a) Wu, S.; Cao, Q.; Wang, X.; Cheng, K.; Cheng, Z. Design, synthesis and biological evaluation of mitochondria targeting theranostic agents. *Chem. Commun.* **2014**, *50*, 8919–8922. (b) Luo, S.; Tan, X.; Fang, S.; Wang, Y.; Liu, T.; Wang, X.; Yuan, Y.; Sun, H.; Qi, Q.; Shi, C. Mitochondria-Targeted Small-Molecule Fluorophores for Dual Modal Cancer Phototherapy. *Adv. Funct. Mater.* **2016**, *26*, 2826–2835. (c) Gao, P.; Pan, W.; Li, N.; Tang, B. Fluorescent probes for organelle-targeted bioactive species imaging. *Chem. Sci.* **2019**, *10*, 6035–6071.
- (10) (a) Wagner, N.; Stephan, M.; Höglinger, D.; Nadler, A. A Click cage: Organelle-specific uncaging of lipid messengers. *Angew. Chem. Int. Ed.* **2018**, *57*, 13339–13343. (b) Kand, D.; Pizarro, L.; Angel, I.; Avni, A.; Friedmann-Morvinski, D.; Weinstein, R. Organelle-targeted BODIPY photocages: Visible-light-mediated subcellular photorelease. *Angew. Chem. Int. Ed.* **2019**, *58*, 4659–4663.
- (11) Gandioso, A.; Bresolí-Obach, R.; Nin-Hill, A.; Bosch, M.; Palau, M.; Galindo, A.; Contreras, S.; Rovira, A.; Rovira, C.; Nonell, S.; Marchán, V. Redesigning the coumarin scaffold into small bright fluorophores with far-red to near-infrared emission and large Stokes shifts useful for cell imaging. *J. Org. Chem.* **2018**, *83*, 1185–1195.
- (12) Gandioso, A.; Palau, M.; Bresolí-Obach, R.; Galindo, A.; Rovira, A.; Bosch, M.; Nonell, S.; Marchán, V. High photostability in nonconventional coumarins with far-red/NIR emission through azetidinylation. *J. Org. Chem.* **2018**, *83*, 11519–11531.
- (13) Rovira, A.; Gandioso, A.; Goñalons, M.; Galindo, A.; Massaguer, A.; Bosch, M.; Marchán, V. Solid-phase approaches for labeling targeting peptides with far-red emitting coumarin fluorophores. *J. Org. Chem.* **2019**, *84*, 1808–1817.
- (14) Novohradsky, V.; Rovira, A.; Hally, C.; Galindo, A.; Vigueras, G.; Gandioso, A.; Svitelova, M.; Bresolí-Obach, R.; Kostyunova, H.; Markova, L.; Kasparkova, J.; Nonell, S.; Ruiz, J.; Brabec, V.; Marchán, V. Towards novel photodynamic anticancer agents generating superoxide anion radicals: A cyclometalated Ir(III) complex conjugated to a far-red emitting coumarin. *Angew. Chem., Int. Ed.* **2019**, *58*, 6311–6315.



- (15) (a) Gandioso, A.; Palau, M.; Nin-Hill, A.; Melnyk, I.; Rovira, C.; Nonell, S.; Velasco, D.; García-Amorós, J.; Marchán, V. Sequential Uncaging with Green Light can be Achieved by Fine-Tuning the Structure of a Dicyanocoumarin Chromophore. *ChemistryOpen* **2017**, *6*, 375–384. (b) Gandioso, A.; Contreras, S.; Melnyk, I.; Oliva, J.; Nonell, S.; Velasco, D.; García-Amorós, J.; Marchán, V. Development of Green/Red-Absorbing Chromophores Based on a Coumarin Scaffold That Are Useful as Caging Groups. *J. Org. Chem.* **2017**, *82*, 5398–5408.
- (16) Vakuliuk, O.; Jun, Y. W.; Vygranenko, K.; Clermont, G.; Reo, Y. J.; Blanchard-Desce, M.; Ahn, K. H.; Gryko, D. T. Modified Isoindolediones as Bright Fluorescent Probes for Cell and Tissue Imaging. *Chem. – Eur. J.* **2019**, *25*, 13354–13362.
- (17) (a) Magde, D.; Brannon, J. H.; Cremers, T. L.; Olmsted, J. Absolute luminescence yield of cresyl violet. A standard for the red. *J. Phys. Chem.* **1979**, *83*, 696–699. (b) Würth, C.; Grabolle, M.; Pauli, J.; Spieles, M.; Resch-Genger, U. Relative and absolute determination of fluorescence quantum yields of transparent samples. *Nat. Protoc.* **2013**, *8*, 1535–1550. (c) Brouwer, A. M. Standards for photoluminescence quantum yield measurements in solution (IUPAC Technical Report). *Pure Appl. Chem.* **2011**, *83*, 2213–2228.
- (18) Bolte, S.; Cordelières, F. P. A Guided Tour Into Subcellular Colocalization Analysis in Light Microscopy. *J. Microsc.* **2006**, *224*, 213–232.
- (19) Hasumi, K.; Sato, S.; Saito, T.; Kato, J.; Shiota, K.; Sato, J.; Suzuki, H.; Ohta, S. Design and synthesis of 5-[(2-chloro-6-fluorophenyl)acetylamino]-3-(4-fluorophenyl)-4-(4-pyrimidinyl)-isoxazole (AKP-001), a novel inhibitor of p38 MAP kinase with reduced side effects based on the antedrug concept. *Bioorg. Med. Chem.* **2014**, *22*, 4162–4176.
- (20) Schindelin, J.; Arganda-Carreras, I.; Frise, E.; Kaynig, V.; Longair, M.; Pietzsch, T.; Preibisch, S.; Rueden, C.; Saalfeld, S.; Schmid, B.; Tinevez, J. Y.; White, D. J.; Hartenstein, V.; Eliceiri, K.; Tomancak, P.; Cardona, A. Fiji: an open-source platform for biological-image analysis. *Nat. Methods* **2012**, *9*, 676–682.
- (21) Prewitt, J. M. S.; Mendelsohn, M. L. The analysis of cell images. *Ann. N. Y. Acad. Sci.* **1966**, *128*, 1035–1053.
- (22) Phansalkar, N.; More, S.; Sabale, A.; Madhuri, J. Adaptive local thresholding for detection of nuclei in diversity stained cytology images. *International Conference on Communications and Signal Processing (ICCSP)* 2011, 218–220, doi: DOI: 10.1109/ICCSP.2011.5739305.